View metadata, citation and similar papers at core.ac.uk

brought to you by CORE

provided by NASA Technical Reports Server


# The role of compressibility in energy release by magnetic reconnection

J. Birn, J. E. Borovsky, and M. Hesse

Citation: Phys. Plasmas **19**, 082109 (2012); doi: 10.1063/1.4742314
View online: http://dx.doi.org/10.1063/1.4742314
View Table of Contents: http://pop.aip.org/resource/1/PHPAEN/v19/i8
Published by the American Institute of Physics.

## Additional information on Phys. Plasmas

Journal Homepage: http://pop.aip.org/
Journal Information: http://pop.aip.org/about/about_the_journal
Top downloads: http://pop.aip.org/features/most_downloaded
Information for Authors: http://pop.aip.org/authors

ADVERTISEMENT

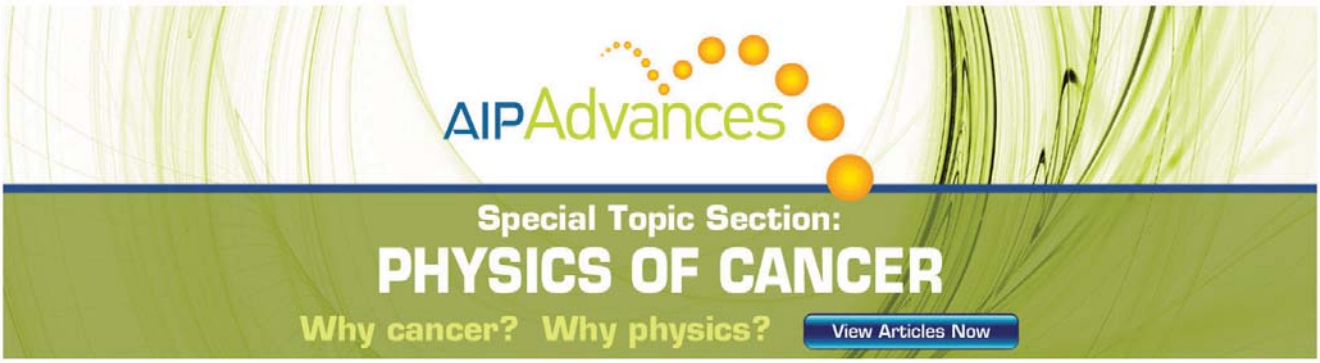


Downloaded 29 Apr 2013 to 128.183.168.225. This article is copyrighted as indicated in the abstract. Reuse of AIP content is subject to the terms at: http://pop.aip.org/about/rights_and_permissions

# The role of compressibility in energy release by magnetic reconnection

J. Birn,[1,a)] J. E. Borovsky,[1] and M. Hesse[2]
[1]*Los Alamos National Laboratory, Los Alamos, New Mexico 87545, USA*
[2]*NASA/Goddard Space Flight Center, Greenbelt, Maryland 20771, USA*

(Received 31 May 2012; accepted 17 July 2012; published online 6 August 2012)

Using resistive compressible magnetohydrodynamics, we investigate the energy release and transfer by magnetic reconnection in finite (closed or periodic) systems. The emphasis is on the magnitude of energy released and transferred to plasma heating in configurations that range from highly compressible to incompressible, based on the magnitude of the background $\beta$ (ratio of plasma pressure over magnetic pressure) and of a guide field in two-dimensional reconnection. As expected, the system becomes more incompressible, and the role of compressional heating diminishes, with increasing $\beta$ or increasing guide field. Nevertheless, compressional heating may dominate over Joule heating for values of the guide field of 2 or 3 (in relation to the reconnecting magnetic field component) and $\beta$ of 5–10. This result stems from the strong localization of the dissipation near the reconnection site, which is modeled based on particle simulation results. Imposing uniform resistivity, corresponding to a Lundquist number of $10^3$ to $10^4$, leads to significantly larger Ohmic heating. Increasing incompressibility greatly reduces the magnetic flux transfer and the amount of energy released, from $\sim$10% of the energy associated with the reconnecting field component, for zero guide field and low $\beta$, to $\sim 0.2\% - 0.4\%$ for large values of the guide field $B_{y0} > 5$ or large $\beta$. The results demonstrate the importance of taking into account plasma compressibility and localization of dissipation in investigations of heating by turbulent reconnection, possibly relevant for solar wind or coronal heating. © *2012 American Institute of Physics*. [http://dx.doi.org/10.1063/1.4742314]

## I. INTRODUCTION

Magnetic reconnection is with little doubt the major mechanism enabling energy release in solar flares and magnetospheric substorms. The standard models of these events involve large volumes but single reconnection sites, where the ideal magnetohydrodynamic (MHD) assumption of frozen-in fields breaks down, typically in the vicinity of a magnetic neutral line (x-line) or separator. In addition to these explosive single site events, reconnection at multiple sites, presumably associated with turbulence, may also be of relevance as a mechanism to heat the solar corona[1] or the solar wind,[2] although direct observational support is hard to obtain.

Theoretically, one might distinguish between reconnection in large or open systems, which do not significantly inhibit the outflow from the reconnection site (such as reconnection at the magnetopause or large-scale solar wind events) and reconnection in confined or quasi-periodic systems, where the limited size provides a constraint on the outflow and thereby on the energy conversion. Interestingly, the standard flare and substorm models are of a mixed type. On one side, toward the Sun or the Earth, the outflow is constrained, with wave propagation and reflection times comparable to the impulsive evolution time. On the other side, away from the Sun or the Earth, the outflow may be considered as uninhibited with no feedback from outgoing waves.

Turbulent reconnection scenarios can be considered as examples of the second kind, for which the limited size of reconnection sites may be relevant for energy release and conversion. Reconnection in MHD turbulence has been examined using incompressible-MHD simulations with non-uniform resistivity,[3] incompressible-MHD simulations with uniform resistivity,[4,5] compressible-MHD simulations with uniform resistivity,[6,7] and by compressible-Hall-MHD simulations with uniform resistivity.[8] The inadequacy of using uniform resistivity has been noted by Lehe *et al.*[7]

In the present paper, we focus on isolated or periodic systems. Earlier investigations[9–11] have demonstrated that plane current sheets of limited size relax, via reconnection, into new equilibria with lower magnetic, but increased thermal energy (with small amounts of excess kinetic energy if the total energy is conserved). The final states were surprisingly similar for MHD, Hall MHD, hybrid, and full particle-in-cell (PIC) simulations. This fact supports a view that differences in the dissipation mechanisms do not strongly affect the final states and the amount of energy released, mainly because the dissipation is strongly localized. Equilibrium approaches[11] further confirmed that the final states are governed by the approximate conservation of mass,

$$M = \int \rho ds/B, \tag{1}$$

and of an entropy-related integral

$$S = \int p^{1/\gamma} ds/B, \tag{2}$$

a)Now at Space Science Institute, Boulder, Colorado 80301, USA. Electronic mail: jbirn@spacescience.org.

 © 2012 American Institute of Physics

Downloaded 29 Apr 2013 to 128.183.168.225. This article is copyrighted as indicated in the abstract. Reuse of AIP content is subject to the terms at: http://pop.aip.org/about/rights_and_permissions

integrated along magnetic flux tubes between boundary intersections. In the simulations, this result stems from the absence of significant (integrated) dissipation, magnetic slippage, and heat flux across the magnetic field. In the MHD simulations, these features are imposed, provided that resistive dissipation, necessary to enable reconnection, is strongly localized. The comparison of the simulation results demonstrated that these properties were also very well satisfied in the particle simulations,[10] despite the operation of reconnection.

The two-dimensional configurations investigated by Zaharia and Birn[11] did not contain a guide field but considered different ranges of compressibility by varying the polytropic index $\gamma$. They found that increasing $\gamma$ towards incompressibility significantly reduced the amount of magnetic energy released and converted to internal, that is, thermal energy. Birn and Hesse[12] extended the investigation to two-dimensional configurations ($\partial/\partial y \equiv 0$) that included a guide field $B_y$, assumed to be either uniform initially or satisfying the force-free condition $\mathbf{J} \times \mathbf{B} = 0$. They showed that the final energy state, in both, MHD and PIC simulations is governed by another approximately conserved quantity for each flux tube

$$Y = \int B_y ds/B, \tag{3}$$

which can be identified as the displacement of footpoints of field lines between two boundary intersections but is also related to helicity.[13] The conservation of $Y$ for each field line (as well as the conservation of $M$ and $S$) provides a much more stringent condition on energy release than the conservation of total helicity within a volume considered.[14]

In this paper, we further investigate the role of compressibility and of a guide field in energy release and transfer by magnetic reconnection. In Sec. II, we present the basic setup and approach. This is followed by fundamental equations governing energy budgets in Sec. III. In Secs. IV and V, we then investigate the influence of resistivity models and compressibility on energy conversion on the basis of resistive MHD simulations. Sections VI and VII address the roles of the integral constraints and the system size, respectively, with a summary and discussion in Sec. VIII.

## II. INITIAL STATES AND NUMERICAL APPROACH

In the following, we will use dimensionless quantities, based on the magnetic field strength of the reconnecting magnetic field component outside the current sheet, $B_x = B_0$, the initial density $\rho_0$, which is assumed to be uniform, and the half-thickness of the current sheet, $L_0$, with other units given by appropriate combinations of these, for instance, velocity $v_0 = B_0/\sqrt{\mu_0\rho_0}$, time $t_0 = L_0/v_0$, pressure $p_0 = B_0^2/\mu_0$, and electric field $E_0 = v_0 B_0$.

The initial current sheet configuration consists of a one-dimensional Harris-type magnetic field profile, given by

$$\begin{aligned} B_x &= \tanh z, \\ B_z &= 0. \end{aligned} \tag{4}$$

The initial state also includes a guide field $B_y$, given by

$$B_y = \sqrt{B_{y0}^2 + p_f/\cosh^2 z}. \tag{5}$$

For $p_f = 0$, the guide field is constant, while $p_f = 1$ represents a force-free state, $B_x^2 + B_y^2 = \text{const}$. Here, we use magnetotail coordinates with $x$ along the field that reverses sign across the current sheet, $z$ perpendicular to the current sheet, and $y$ in the invariant direction.

The corresponding plasma pressure follows from pressure balance; it is given by

$$p = \frac{1}{2}(1 + B_{y0}^2 - B_x^2 - B_y^2 + \beta) = \frac{1}{2}[\beta + (1 - p_f)/\cosh^2 z], \tag{6}$$

where an arbitrary background pressure $p_b = (1/2)\beta$ is included. We note that $\beta$ is defined on the basis of the pressure of the reconnecting magnetic field component outside the current sheet, $B_x = B_0$, not the total magnetic pressure. The plasma density is chosen uniform as

$$\rho = 1. \tag{7}$$

The reconnection problem outlined above was studied by a MHD code,[15] using nonuniform grids with up to $400^2$ grid cells and a localized resistivity model given by

$$\eta = \eta_0 + \eta_1/\cosh^2 r, \quad r = \sqrt{(x/d_x)^2 + (z/d_z)^2}, \tag{8}$$

centered at $x = 0$, $z = 0$. This choice, together with the imposed symmetry, determines the location of the magnetic null (x-point) where $B_x = 0$ and $B_z = 0$. The grid size and the number of grid points were varied to ensure that they did not affect the results.

The scenario considered is similar to the "Newton Challenge" problem,[9] however, without external inflow or driving. Symmetry boundary conditions were employed at $x = L_x$ and at $x = 0$. For most of the runs, the box size was chosen to be twice the size in $z$ as in the Newton challenge problem, given by

$$L_x = 8, \quad L_z = 8. \tag{9}$$

In most cases, the scales for the localized resistivity were chosen as

$$d_x = 0.2, \quad d_z = 0.2. \tag{10}$$

The small size of the resistive spot relative to the box size was chosen in response to comparisons with PIC simulations, which indicated a strong localization of dissipation.[10]

## III. ENERGY BUDGETS

An important element that is used in our analysis is the energy budget, which may be split up into the following three equations for magnetic, internal, and bulk kinetic energy, respectively:[16]

$$\frac{\partial}{\partial t}\frac{B^2}{2} = -\nabla \cdot (\mathbf{E} \times \mathbf{B}) - \mathbf{j} \cdot \mathbf{E}, \tag{11}$$

Downloaded 29 Apr 2013 to 128.183.168.225. This article is copyrighted as indicated in the abstract. Reuse of AIP content is subject to the terms at: http://pop.aip.org/about/rights_and_permissions

$$\frac{\partial u}{\partial t} = -\nabla \cdot [(u+p)\mathbf{v}] + \mathbf{v} \cdot \nabla p + \eta j^2, \tag{12}$$

$$\frac{\partial}{\partial t}\frac{\rho}{2}v^2 = -\nabla \cdot \left(\frac{\rho}{2}v^2\mathbf{v}\right) + \mathbf{v} \cdot (\mathbf{j} \times \mathbf{B} - \nabla p), \tag{13}$$

where $u = p/(\gamma - 1)$ is the internal (thermal) energy density, and $\mathbf{E} = -\mathbf{v} \times \mathbf{B} + \eta \mathbf{j}$ in resistive MHD, such that $\mathbf{j} \cdot \mathbf{E} = -\mathbf{j} \cdot (\mathbf{v} \times \mathbf{B}) + \eta j^2$, and $\gamma$ is the ratio of specific heats with $\gamma = 5/3$ for an isotropic plasma pressure.

The terms to the right of the divergence terms in Eqs. (11)–(13) describe the transfer of one form of energy to another; the sum of these vanishes. There are three different transfer terms. The first one is Joule dissipation, equivalent to Ohmic heating $\eta j^2$ in the resistive MHD model. The second term, $-\mathbf{j} \cdot (\mathbf{v} \times \mathbf{B}) = \mathbf{v} \cdot (\mathbf{j} \times \mathbf{B})$, represents acceleration (or deceleration) by Lorentz forces as a mechanism of transfer between magnetic and bulk kinetic energy, while the third term, $\mathbf{v} \cdot \nabla p$, provides the transfer between bulk kinetic energy and thermal energy, representing work done by pressure forces. In approximate force balance, $\mathbf{j} \times \mathbf{B} \approx \nabla \cdot \mathbf{P}$, the combination of these two terms also provide a mechanism of transfer between magnetic and thermal energy. This is in fact how compressional heating may transfer magnetic to thermal energy, also in collisionless plasmas. While this is in principle a reversible process, it may contribute to irreversible heating when combined with the unidirectional transport from inflow to outflow in magnetic reconnection events.

In the present paper, we are particularly interested in the total amounts of energy released and transferred. These can be written as

$$\Delta W_{mag} = \int_0^t \int \frac{B^2}{2} dF dt = -\Delta W_L - \Delta W_{ohm}, \tag{14}$$

$$\Delta W_{int} = \int_0^t \int u\, dF dt = \Delta W_{comp} + \Delta W_{ohm}, \tag{15}$$

$$\Delta W_{kin} = \int_0^t \int \frac{\rho v^2}{2} dF dt = \Delta W_L - \Delta W_{comp}, \tag{16}$$

where

$$\Delta W_{ohm} = \int_0^t \int \eta j^2\, dF dt, \tag{17}$$

$$\Delta W_L = \int_0^t \int \mathbf{v} \cdot (\mathbf{j} \times \mathbf{B})\, dF dt, \tag{18}$$

$$\Delta W_{comp} = \int_0^t \int \mathbf{v} \cdot \nabla p\, dF dt = -\int_0^t \int p \nabla \cdot \mathbf{v}\, dF dt. \tag{19}$$

Here, the integrals $\int dF = \int dx\, dz$ are taken over the entire box, such that the integrals over the divergence terms vanish for closed or periodic boundary conditions.

## IV. CHARACTERISTIC EVOLUTION AND RESISTIVITY DEPENDENCE

Figure 1 illustrates the evolution of magnetic, internal, and kinetic energy for a run with $B_{y0} = 1$ and $\beta = 0.2$, using

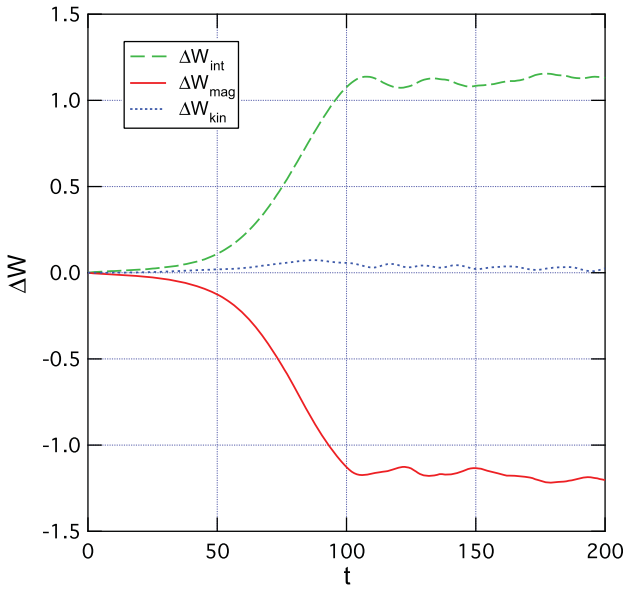


FIG. 1. Evolution of energy changes (bottom) for a run with a localized resistivity given by Eq. (8) with $\eta_1 = 0.02, d_x = 0.2, d_z = 0.2$, showing magnetic energy (solid line), internal (thermal) energy (dashed line), and bulk kinetic energy (dotted line).

localized resistivity (8) with $\eta_0 = 0$ and $\eta_1 = 0.02, d_x = 0.2$, $d_z = 0.2$. After $t \approx 100$, a near equilibrium is reached. It is remarkable that only very little energy is converted to (bulk) kinetic energy. This is consistent with earlier results from reconnection in a finite box of relatively small size,[10,12] but in contrast to reconnection in open or steady state models,[17,18] in which roughly one half of the magnetic energy released goes into kinetic energy flux, while the other half goes into enthalpy flux (consisting of convected thermal energy plus the work done by pressure gradients).

Due to the smallness of the net energy going into kinetic energy, the final states are very close to an equilibrium, with only minor oscillations. These final states are illustrated in Fig. 2, obtained at $t = 200$ for three runs with resistivity models given by Eq. (8) with (top) $\eta_0 = 0, \eta_1 = 0.2$, (center) $\eta_0 = 10^{-4}, \eta_1 = 0.2$, and (bottom) $\eta_0 = 10^{-3}, \eta_1 = 0.2$, all with $d_x = 0.2, d_z = 0.2$ and $B_{y0} = 1, \beta = 0.2$. While the results for $\eta_0 = 10^{-4}$ are very similar to those for $\eta_0 = 0$, the results for $\eta_0 = 10^{-3}$ show clear effects of diffusion of $B_y$ and $J_y$.

This effect also shows in the energy changes, demonstrated in Fig. 3 for the internal energy (green lines) and its contributions from compression (blue) and Ohmic heating (red). Fig. 3 shows results from four runs with resistivity models given by Eq. (8), with $\eta_0 = 0, \eta_1 = 0.02$ (solid lines), $\eta_0 = 0, \eta_1 = 0.2$ (dashed lines), $\eta_0 = 10^{-4}, \eta_1 = 0.2$ (dashed-dotted lines), and $\eta_0 = 10^{-3}, \eta_1 = 0.2$ (dotted lines), all with $d_x = 0.2, d_z = 0.2$ and $B_{y0} = 1, \beta = 0.2$.

Fig. 3 shows several remarkable results. Comparing the two cases with $\eta_0 = 0$ (solid lines and dashed lines), we find that the magnitude of the peak resistivity $\eta_1$ localized at the reconnection site has very little influence on the relative amounts of integrated Ohmic and compressional heating. In either case, the compressional heating clearly dominates Ohmic heating. However, the uniform background resistivity

Downloaded 29 Apr 2013 to 128.183.168.225. This article is copyrighted as indicated in the abstract. Reuse of AIP content is subject to the terms at: http://pop.aip.org/about/rights_and_permissions

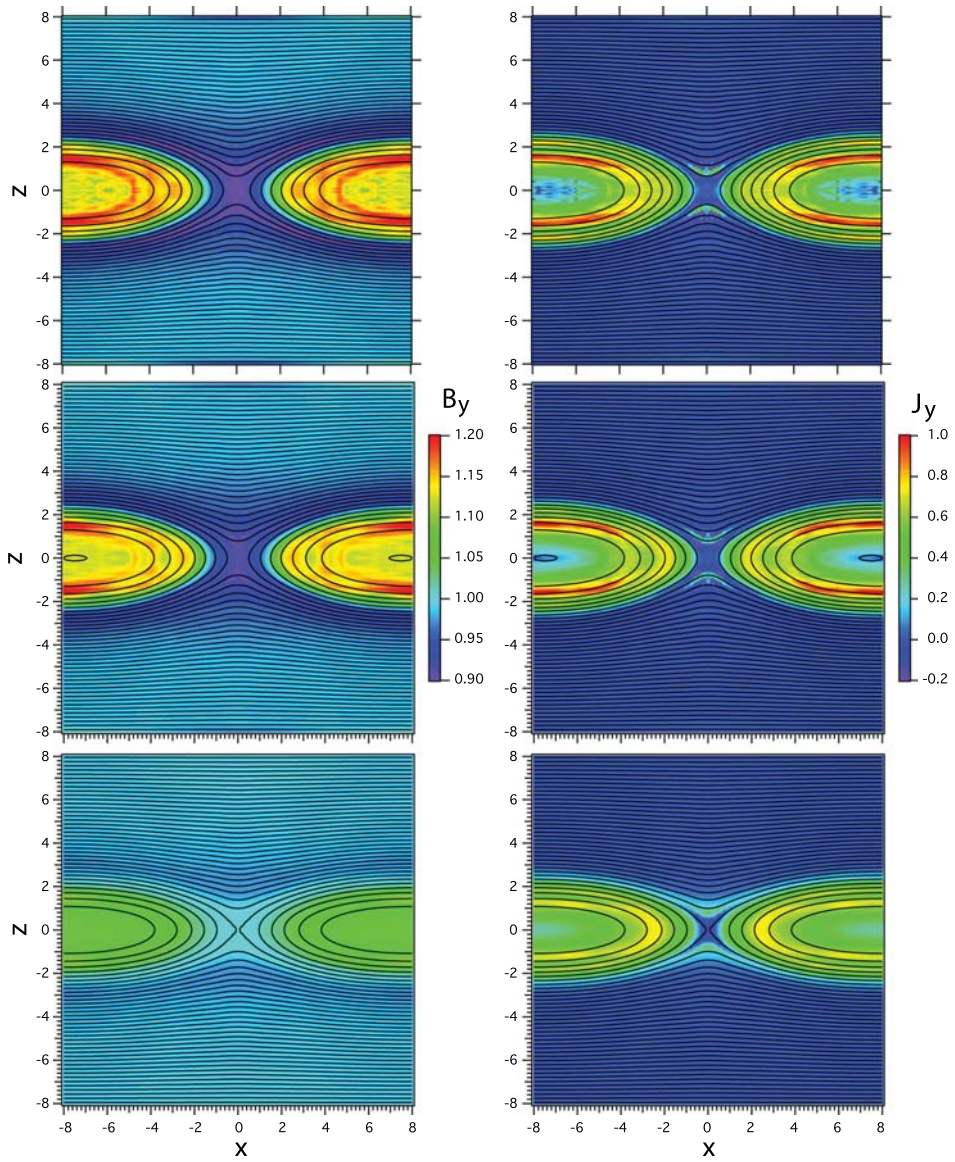


FIG. 2. Late stages of guide field $B_y$ (left) and current density $J_y$ (right) for three runs with resistivity models given by Eq. (8), (top) with $\eta_0 = 0, \eta_1 = 0.2$, (center) $\eta_0 = 10^{-4}, \eta_1 = 0.2$, and (bottom) $\eta_0 = 10^{-3}, \eta_1 = 0.2$, all with $d_x = 0.2, d_z = 0.2$ and $B_{y0} = 1, \beta = 0.2$.

$\eta_0$ can significantly increase the amount of Ohmic heating; even with a small amount of background resistivity ($\eta_0 = 10^{-3}$), the total amount of Ohmic heating swamps the localized Ohmic heating from reconnection and the compressional heating. Also the Ohmic heating continues after the rise from the early fast reconnection. This heating is obviously due to the dissipation of the current that becomes concentrated in the rings within the magnetic islands formed by reconnection (Fig. 2). Even for $\eta_0 = 10^{-4}$ (dashed-dotted red line), the total amount of Ohmic heating from this dissipation exceeds that from reconnection (dashed red line) by a factor of $\sim 3$ at $t = 200$.

## V. EFFECTS OF INCREASING INCOMPRESSIBILITY

Section IV showed results obtained for relatively small $\beta = 0.2$ and moderate guide field magnitude of $B_{y0} = 1$. The investigation of Zaharia and Birn[11] showed that compressibility can have a significant effect on the total amount of magnetic energy released: with increasing incompressibility, modeled formally by increasing $\gamma$, the amount of released energy greatly diminishes. In this section, we investigate the release and conversion of energy, including the relative contributions from Ohmic and compressional heating, using a more physical approach to incompressibility, either increasing $\beta$ or increasing the guide field $B_{y0}$. The former case can be considered as equivalent to increasing $\gamma$ as it increases the ratio between sound speed and Alfvén speed.

Fig. 4 shows the energy changes, obtained at $t = 200$, as functions of $\beta$ for four runs with resistivity models given by Eq. (8), with $\eta_0 = 0, \eta_1 = 0.02$ (solid lines), $\eta_0 = 0, \eta_1 = 0.2$ (dashed lines), $\eta_0 = 10^{-4}, \eta_1 = 0.2$ (dashed-dotted lines), and $\eta_0 = 10^{-3}, \eta_1 = 0.2$ (dotted lines), all with $d_x = 0.2, d_z = 0.2$ and $B_{y0} = 1$. Green lines show the changes of internal energy, consisting of compressional (blue lines) and Ohmic contributions (red).

Fig. 4 confirms the result of Zaharia and Birn[11] that the amount of energy converted to thermal energy, essentially equivalent to the amount of magnetic energy released, decreases significantly with increasing incompressibility, that is, increasing $\beta$. Fig. 4 also shows that, for $\eta_0 = 0$, compressional heating remains dominant up to $\beta \approx 10$. The

Downloaded 29 Apr 2013 to 128.183.168.225. This article is copyrighted as indicated in the abstract. Reuse of AIP content is subject to the terms at: http://pop.aip.org/about/rights_and_permissions

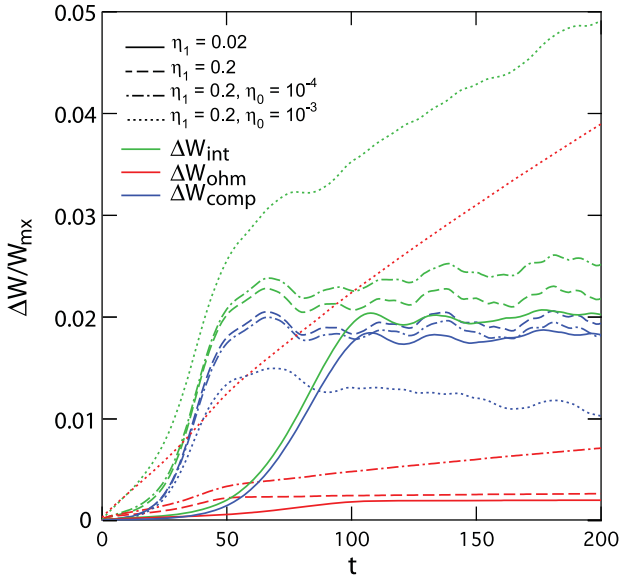


FIG. 3. Evolution of energy changes for the four runs with resistivity models given by Eq. (8), with $\eta_0 = 0$, $\eta_1 = 0.02$ (solid lines), $\eta_0 = 0$, $\eta_1 = 0.2$ (dashed lines), $\eta_0 = 10^{-4}, \eta_1 = 0.2$ (dashed-dotted lines), and $\eta_0 = 10^{-3}$, $\eta_1 = 0.2$ (dotted lines), all with $d_x = 0.2, d_z = 0.2$ and $B_{y0} = 1$, $\beta = 0.2$. Green lines show the change of internal energy, consisting of compressional (blue lines) and Ohmic contributions (red).

threshold becomes reduced, however, when uniform resistivity is added, to $\beta \approx 3$ for $\eta_0 = 10^{-4}$, while for $\eta = 10^{-3}$ Ohmic heating dominates at all values of $\beta$ investigated here.

Similar results are obtained for increasing guide field $B_{y0}$. Fig. 5 shows the energy changes, obtained at $t = 200$, as function of $B_{y0}$ for four runs with resistivity models given by

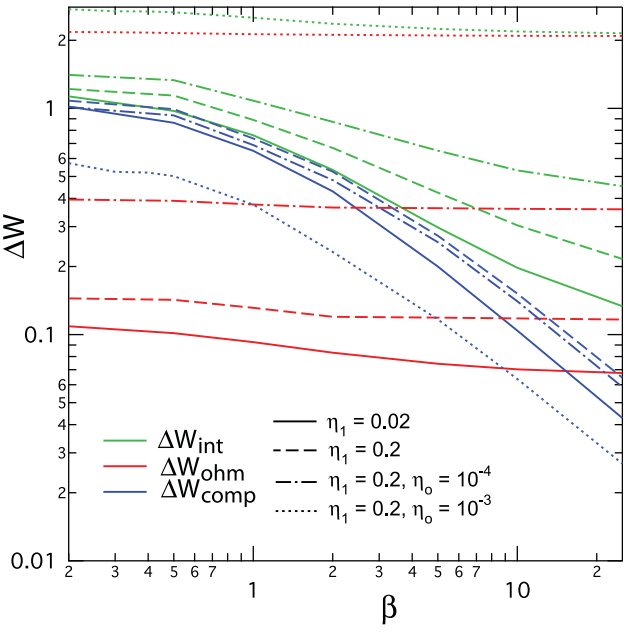


FIG. 4. Energy changes as function of $\beta$ for four runs with resistivity models given by Eq. (8), with $\eta_0 = 0, \eta_1 = 0.02$ (solid lines), $\eta_0 = 0, \eta_1 = 0.2$ (dashed lines), $\eta_0 = 10^{-4}, \eta_1 = 0.2$ (dashed-dotted lines), and $\eta_0 = 10^{-3}, \eta_1 = 0.2$ (dotted lines), all with $d_x = 0.2, d_z = 0.2$ and $B_{y0} = 1$. Green lines show the changes of internal energy, consisting of compressional (blue lines) and Ohmic contributions (red).

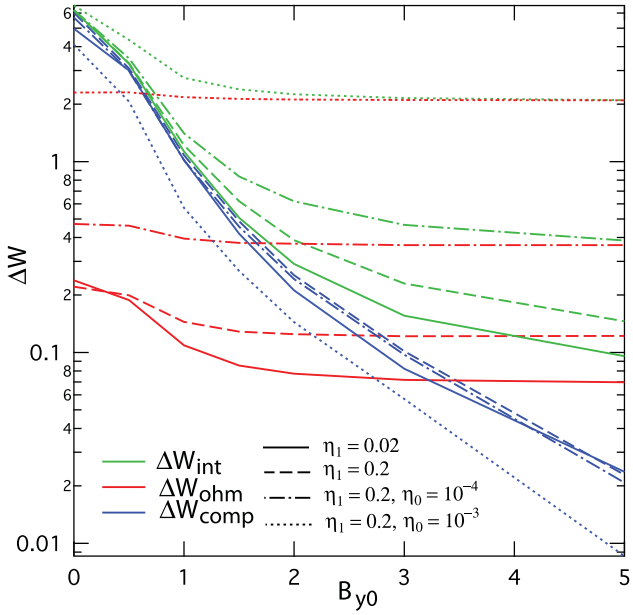


FIG. 5. Energy changes as function of the guide field $B_{y0}$ for four runs with resistivity models given by Eq. (8), with $\eta_0 = 0, \eta_1 = 0.02$ (solid lines), $\eta_0 = 0, \eta_1 = 0.2$ (dashed lines), $\eta_0 = 10^{-4}, \eta_1 = 0.2$ (dashed-dotted lines), and $\eta_0 = 10^{-3}, \eta_1 = 0.2$ (dotted lines), all with $d_x = 0.2, d_z = 0.2$ and $\beta = 0.2$. Green lines show the changes of internal energy, consisting of compressional (blue lines) and Ohmic contributions (red).

Eq. (8), with $\eta_0 = 0, \eta_1 = 0.02$ (solid lines), $\eta_0 = 0, \eta_1 = 0.2$ (dashed lines), $\eta_0 = 10^{-4}, \eta_1 = 0.2$ (dashed-dotted lines), and $\eta_0 = 10^{-3}, \eta_1 = 0.2$ (dotted lines), all with $d_x = 0.2$, $d_z = 0.2$ and $\beta = 0.2$. As before, green lines show the changes of internal energy, with compressional contributions in blue and Ohmic contributions in red. Again, increasing incompressibility, expected from increasing guide field,

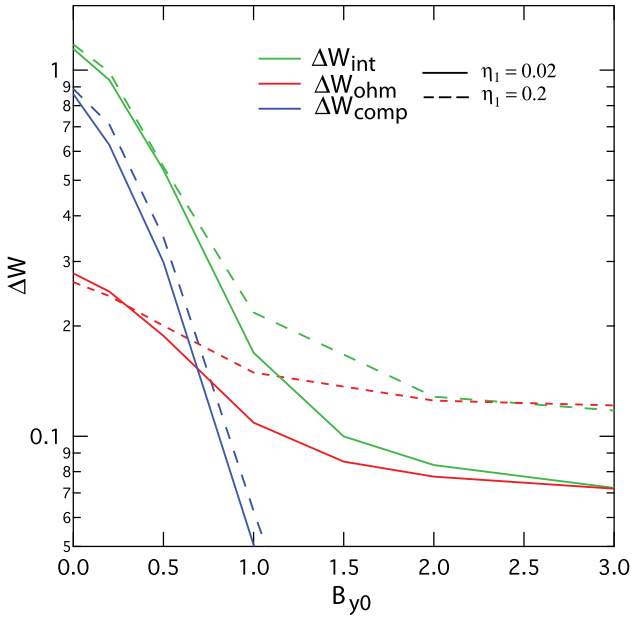


FIG. 6. Energy changes as function of the guide field $B_{y0}$ for two, initially force-free, runs with resistivity models given by Eq. (8), with $\eta_0 = 0, \eta_1 = 0.02$ (solid lines) and $\eta_0 = 0, \eta_1 = 0.2$ (dashed lines), both with $d_x = 0.2, d_z = 0.2$ and $\beta = 0.2$. Green lines show the changes of internal energy, consisting of compressional (blue lines) and Ohmic contributions (red).

Downloaded 29 Apr 2013 to 128.183.168.225. This article is copyrighted as indicated in the abstract. Reuse of AIP content is subject to the terms at: http://pop.aip.org/about/rights_and_permissions

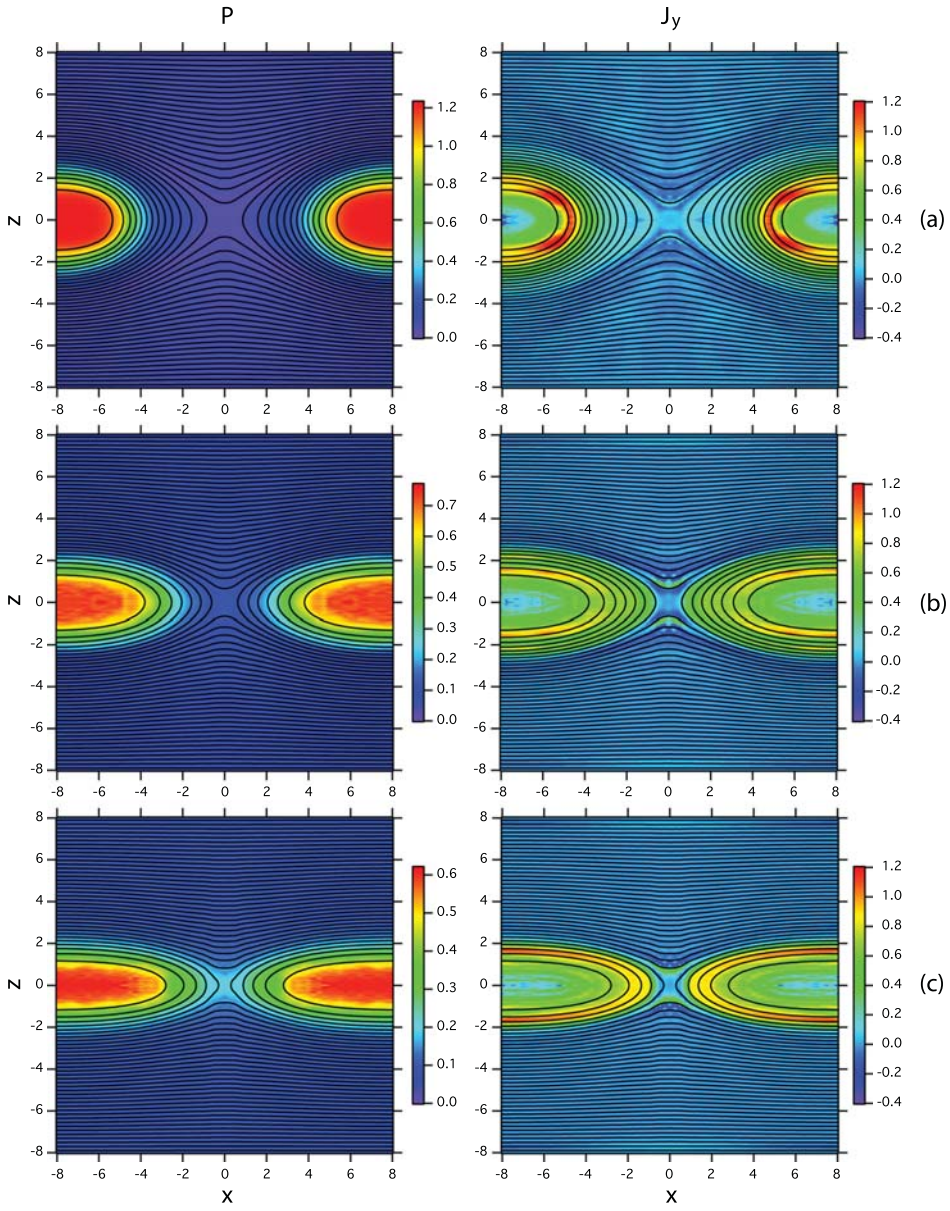


FIG. 7. Late stages of pressure $P$ (left) and current density $J_y$ (right) for three runs with $\eta_0 = 0, \eta_1 = 0.2$, $d_x = 0.2$, $d_z = 0.2$, $\beta = 0.2$ and (a) $B_{y0} = 0$, (b) $B_{y0} = 1$, (c) $B_{y0} = 5$.

reduces the amount of energy released and converted to heat. For $\eta_0 = 0$, compressional heating remains dominant up to $B_{y0} \approx 3$. The threshold again becomes reduced when uniform resistivity is added to $\beta \approx 2$ for $\eta_0 = 10^{-4}$ and $\beta \approx 0.5$ for $\eta = 10^{-3}$.

So far, we have considered only cases with uniform guide field. For some applications, however, such as coronal heating by reconnection, the fields undergoing reconnection may be considered as (nearly) force-free, that is, $\mathbf{j} \times \mathbf{B} \approx \mathbf{0}$, consistent with low $\beta$ even within the current sheet. In that case, a one-dimensional equilibrium is given by Eqs. (4) and (5) with $p_f = 1$, satisfying $|\mathbf{B}| = \text{const}$. Fig. 6 shows the energy changes for two initially force-free cases with $\eta_0 = 0, \eta_1 = 0.02$ (solid lines), $\eta_0 = 0, \eta_1 = 0.2$ (dashed lines) and both with $d_x = 0.2, d_z = 0.2$ and $\beta = 0.2$. Qualitatively, we find the same results as for uniform guide field with decreasing energy release for increasing $B_{y0}$. However, the compressional contribution falls off more rapidly with increasing $B_{y0}$, such that Ohmic heating becomes dominant already for $B_{y0} > 0.7$, corresponding to a guide field in the center of the current sheet of $\sim 1.2$.

## VI. INTEGRAL CONSTRAINTS

The limitation of flux and energy transfer stems from the fact that the evolution leads to final states that are governed by the approximate conservation of the integral quantities $M(A)$, $S(A)$, $Y(A)$, given by Eqs. (1)–(3), where $A$ represents the flux variable ($y$ component of the vector potential), which identifies magnetic field lines. The differences between the late stages are demonstrated by Figure 7 for three runs with $\eta_0 = 0, \eta_1 = 0.2$, $d_x = 0.2, d_z = 0.2$, $\beta = 0.2$ and (a) $B_{y0} = 0$, (b) $B_{y0} = 1$, (c) $B_{y0} = 5$. It is obvious that more flux is reconnected for larger compressibility (smaller $B_{y0}$). The larger compression is also obvious from the increase in the maximum pressure, which was initially 0.6.

Downloaded 29 Apr 2013 to 128.183.168.225. This article is copyrighted as indicated in the abstract. Reuse of AIP content is subject to the terms at: http://pop.aip.org/about/rights_and_permissions

The approximate conservation of mass, entropy, and footpoint displacement as functions of the flux variable $A$, defined by Eqs. (1)–(3), is demonstrated by Fig. 8 for two cases with $B_{y0} = 0$ (blue dashed-dotted lines) and $B_{y0} = 5$ (red solid lines). Black dashed lines show the initial distributions. All runs were based on $\eta_0 = 0, \eta_1 = 0.2,\ d_x = 0.2,$ $d_z = 0.2$. We note that the little peaks indicate the flux value at the x-line, $A = A_0$. This peak results from the fact that the flux tube volume diverges on field lines connecting to a regular magnetic null (in $x$, $z$ coordinates). Flux values $A < A_0$ correspond to reconnected field lines inside the magnetic islands. The shift of this peak to higher $A$ values for the $B_{y0} = 0$ (blue) curves is a further indication that reconnection stops at lower flux values for larger guide field, i.e., larger incompressibility.

Due to the strong localization of resistivity, the integrated entropy (Fig. 8(b)) does not show any significant enhancement. This changes when uniform resistivity is added. Fig. 9 shows the entropy per mass $S(A)/M(A)$ for the two cases with (a) $\eta_0 = 10^{-4}$ and (b) $\eta_0 = 10^{-3}$ presented in Figs. 2–5 (both with $\eta_1 = 0.2,\ d_x = 0.2, d_z = 0.2,\ \beta = 0.2$ and $B_{y0} = 1$). For $\eta_0 = 10^{-4}$, the entropy enhancement is still small but for $\eta_0 = 10^{-3}$, it is considerable, continuously increasing even after reconnection.

## VII. EFFECTS OF THE SYSTEM SIZE

An important factor in evaluating the efficiency of multiple reconnection events in the plasma heating is how closely packed the reconnection sites are. Here, we do not consider that closely packed sites may also enhance the efficiency when the outflow from one site drives the inflow into another site but still consider the sites as independent but limited by their size. In this part of our study, we keep the 2D approximation with the length along the current sheet fixed but vary the extent perpendicular to the current sheet. Fig. 10 shows the amount of energy converted to internal energy as function of the system size $L_z$, (top) for the total amount, (bottom) in relation to the magnetic energy content $W_{mx}$ associated with the reconnecting magnetic field component $B_x$. Figure 10 demonstrates that the total energy release and conversion saturates at a system width of approximately $z_m = 10 - 20$. However, the relative energy gain maximizes at $z_m = 4 - 6$ in the absence of a guide field, while for large guide field the smallest size results in the largest relative energy gain. However, at $\sim 0.8\%$, this is significantly lower than the energy gain in antiparallel reconnection, which maximizes at $\sim 15\%$.

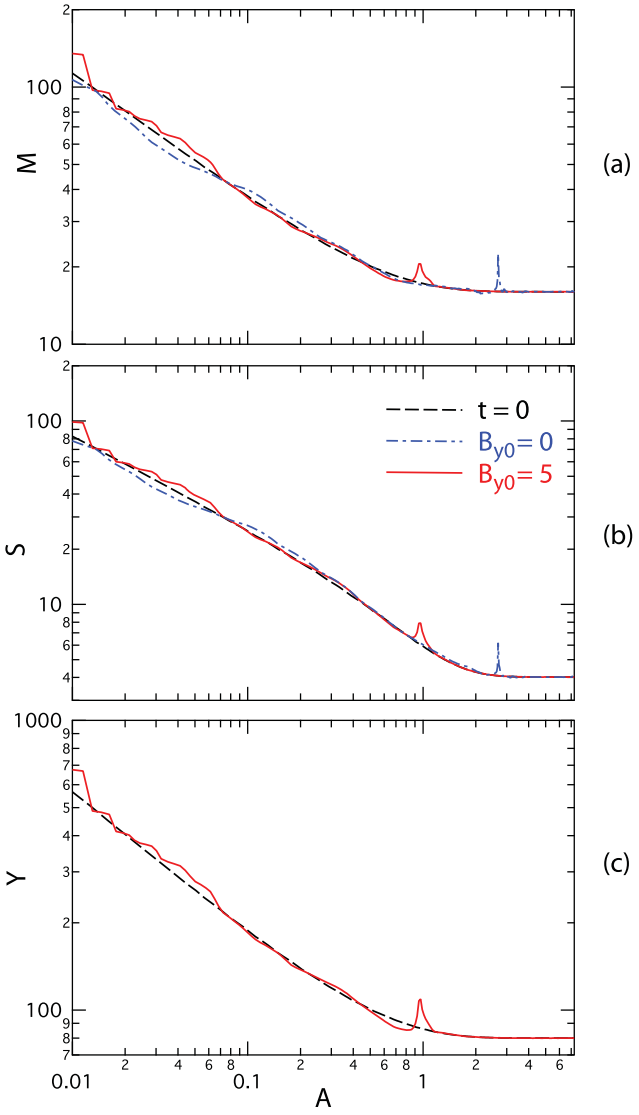


FIG. 8. (a) Mass $M(A)$, (b) entropy function $S(A)$, and (c) footpoint displacement $Y(A)$ as functions of the flux variable $A$, for two runs with $\eta_0 = 0, \eta_1 = 0.2,\ d_x = 0.2, d_z = 0.2,\ \beta = 0.2$ and $B_{y0} = 0$ (blue dashed-dotted lines), $B_{y0} = 5$ (red solid lines). Black dashed lines show the initial distributions.

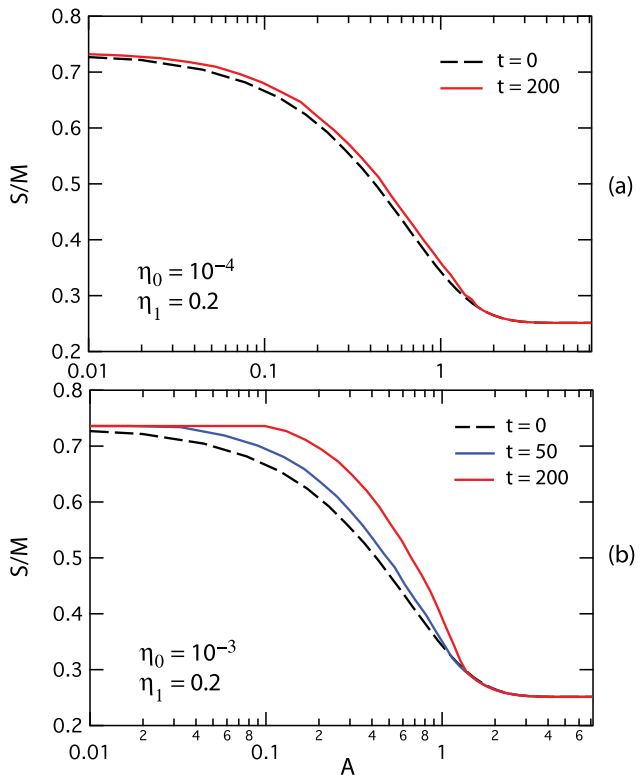


FIG. 9. Entropy per mass $S(A)/M(A)$ for two runs with (a) $\eta_0 = 10^{-4}$ and (b) $\eta_0 = 10^{-3}$, both with $\eta_1 = 0.2,\ d_x = 0.2, d_z = 0.2,\ \beta = 0.2$ and $B_{y0} = 1$. Black dashed lines show the initial distributions.

Downloaded 29 Apr 2013 to 128.183.168.225. This article is copyrighted as indicated in the abstract. Reuse of AIP content is subject to the terms at: http://pop.aip.org/about/rights_and_permissions

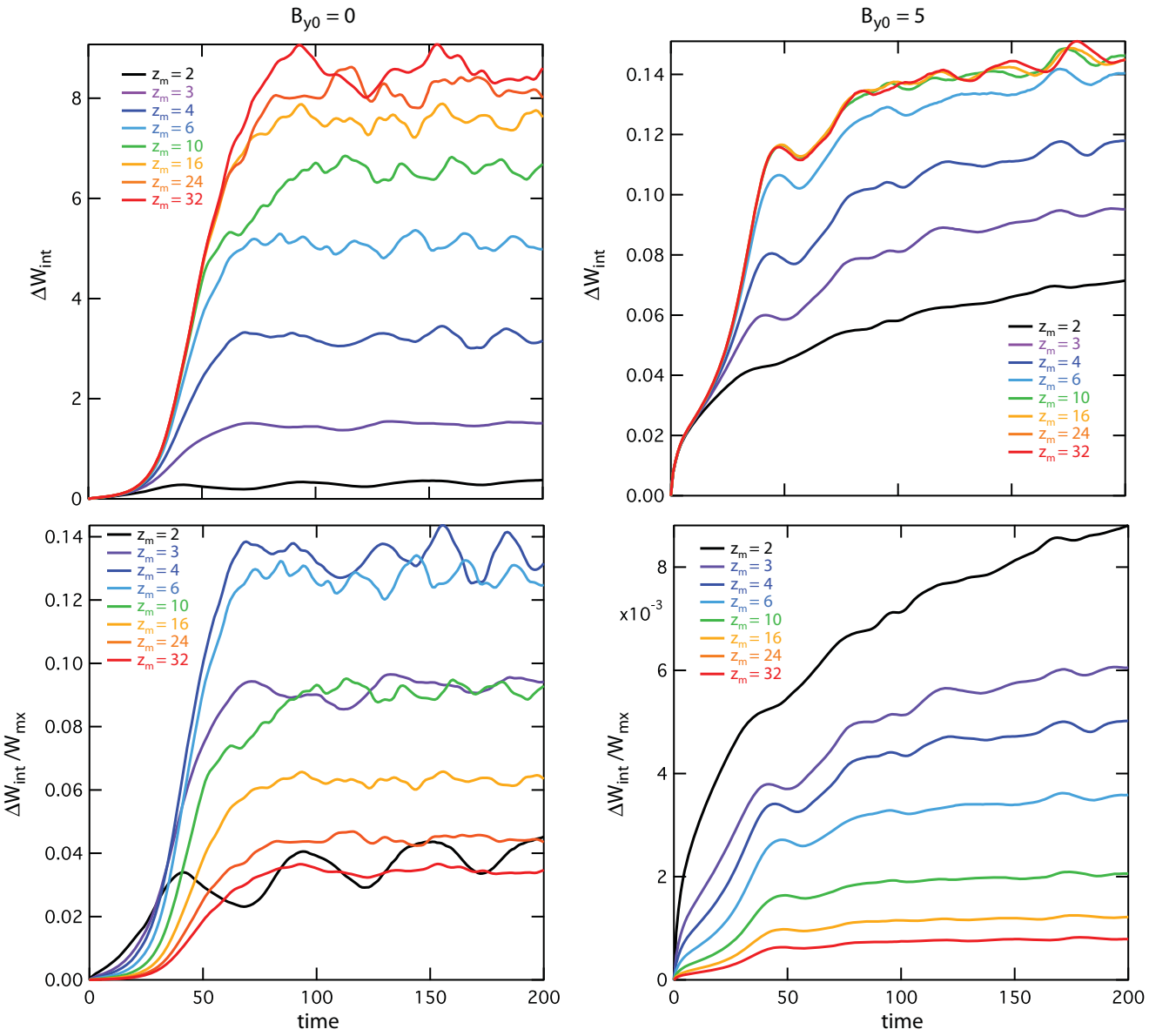


FIG. 10. Internal energy gain as function of time for various system sizes and two values of the guide field, (left) $B_{y0} = 0$, (right) $B_{y0} = 5$.

## VIII. SUMMARY AND CONCLUSIONS

Using resistive MHD simulations, we have investigated energy release and transfer by reconnection in finite (closed or periodic) systems. The emphasis was on the total amount of energy released and transferred to plasma heating in configurations that range from highly compressible to nearly incompressible, based on the magnitude of the background $\beta$ (ratio of plasma pressure over magnetic pressure) and of a guide field in two-dimensional reconnection.

As expected, the system becomes more incompressible, and the role of compressional heating diminishes, with increasing $\beta$ and increasing guide field. Nevertheless, compressional heating may dominate over Joule heating for values of the guide field of 2 or 3 and $\beta$ of 5–10 (based on the magnitude and the pressure of the reconnecting magnetic field component). This result stems from the strong localization of the dissipation near the reconnection site, which is modeled based on particle simulation results. Imposing uniform resistivity, corresponding to Lundquist (or magnetic Reynolds) numbers $R_m$ of $10^3$ to $10^4$ (or $\sim 10^4 - 10^5$ if based on the length of the current sheet rather than its half-thickness), leads to significantly larger Ohmic heating. This heating, however, does not stem from reconnection but from the continued dissipation of current that collects within magnetic islands or flux ropes after reconnection.

Consistent with earlier findings, obtained for varying $\gamma$,[11] we find that the amount of energy released by reconnection and converted to heat greatly diminishes with increasing incompressibility. For a guide field strength of 5, only $\sim 0.3\%$ of the magnetic energy of the reconnecting magnetic field gets converted to heat with similar results for large $\beta$. The limitation of the energy released (and similarly of the magnetic flux reconnected) stems from the constraints imposed on the final states by the approximate conservation of mass $M(A)$, entropy

Downloaded 29 Apr 2013 to 128.183.168.225. This article is copyrighted as indicated in the abstract. Reuse of AIP content is subject to the terms at: http://pop.aip.org/about/rights_and_permissions

$S(A)$, and foot point displacement $Y(A)$, which is related to the integrated helicity, not just for the entire box but for each flux tube. This approximate conservation is closely related to the strong localization of dissipation. The results demonstrate the importance of taking account compressibility and localization of dissipation in investigations of energy release and transfer by turbulent reconnection, possibly relevant for solar wind or coronal heating.

## ACKNOWLEDGMENTS

This work was performed under the auspices of the U.S. Department of Energy, supported by grants from NASA's Supporting Research and Technology and MMS/SMART Programs. The authors acknowledge stimulating discussions with S. Boldyrev and J. C. Perez.

[1]E. R. Priest, in *Reconnection of Magnetic Fields*, edited by J. Birn and E. R. Priest (Cambridge University Press, Cambridge, UK, 2007), pp. 229–237.
[2]R. J. Leamon, W. H. Matthaeus, C. W. Smith, G. P. Zank, D. J. Mullan, and S. Oughton, Astrophys. J. **537**, 1045 (2000).
[3]D. Biskamp and U. Bremer, Phys. Rev. Lett. **72**, 3819 (1993).
[4]M. Wan, S. Oughton, S. Servidio, and W. H. Matthaeus, Phys. Plasmas **17**, 082308 (2010).
[5]S. Servidio, A. Greco, W. H. Matthaeus, K. T. Osman, and P. Dmitruk, J. Geophys. Res. **116**, A09102, doi:10.1029/2011JA016569 (2011).
[6]P. Dmitruk, W. H. Matthaeus, and N. Seenu, Astrophys. J. **617**, 667 (2004).
[7]R. Lehe, I. J. Parrish, and E. Quataert, Astrophys. J. **707**, 404 (2009).
[8]P. Dmitruk and W. H. Matthaeus, Phys. Plasmas **13**, 042307 (2006).
[9]J. Birn, K. Galsgaard, M. Hesse, M. Hoshino, J. Huba, G. Lapenta, P. L. Pritchett, K. Schindler, L. Yin, J. Büchner, T. Neukirch, and E. R. Priest, Geophys. Res. Lett. **32**, L06105, doi:10.1029/2004GL022058 (2005).
[10]J. Birn, M. Hesse, and K. Schindler, Phys. Plasmas **13**, 092117 (2006).
[11]S. Zaharia and J. Birn, Phys. Plasmas **14**, 07210 (2007).
[12]J. Birn and M. Hesse, Phys. Plasmas **17**, 012109 (2010).
[13]J. Birn, M. Hesse, K. Schindler, and S. Zaharia, J. Geophys. Res. **15**, A00D03, doi:10.1029/2008JA014015 (2009).
[14]M. A. Berger and G. B. Field, J. Fluid Mech. **147**, 133 (1984).
[15]J. Birn, F. Iinoya, J. U. Brackbill, and M. Hesse, Geophys. Res. Lett. **23**, 323, doi:10.1029/95GL03857 (1996).
[16]J. Birn and M. Hesse, Ann. Geophys. **23**, 3365 (2005).
[17]E. R. Priest and T. G. Forbes, *Magnetic Reconnection: MHD Theory and Applications* (Cambridge University Press, Cambridge, 2000).
[18]J. Birn, J. E. Borovsky, M. Hesse, and K. Schindler, "Scaling of asymmetric reconnection in compressible plasmas," Phys. Plasmas **17**, 052108 (2010).

Downloaded 29 Apr 2013 to 128.183.168.225. This article is copyrighted as indicated in the abstract. Reuse of AIP content is subject to the terms at: http://pop.aip.org/about/rights_and_permissions